A novel analytical model to characterise the monotonic and cyclic contribution of fibre bridging during Mode I fatigue delamination in (C)FRPs

Monticeli, Francisco; Biagini, Davide; Mosleh, Yasmine; Pascoe, John-Alan

DOI
10.1016/j.compositesb.2025.112319

Publication date
2025

Document Version
Final published version

Published in
Composites Part B: Engineering

Composites Part B 297 (2025) 112319

Contents lists available at ScienceDirect

Composites Part B

journal homepage: www.elsevier.com/locate/compositesb

A novel analytical model to characterise the monotonic and cyclic contribution of fibre bridging during Mode I fatigue delamination in (C)FRPs

Francisco Maciel Monticeli [a,*], Davide Biagini [a], Yasmine Mosleh [b], John-Alan Pascoe [a]

[a] Department of Aerospace Structures and Materials, Faculty of Aerospace Engineering, Delft University of Technology, Kluyverweg 1, 2629 HS, Delft, the Netherlands
[b] Department of Engineering Structures, Faculty of Civil Engineering and Geosciences, Delft University of Technology, Stevinweg 1, 2628 CN, Delft, the Netherlands

ARTICLE INFO

Handling Editor: Prof. Ole Thomsen

Keywords:
Composite materials
Fatigue
Fibre bridging
Delamination

ABSTRACT

Fibre bridging is an important phenomenon influencing the mode I delamination growth behaviour in composite materials. Accurate modelling of this phenomenon is required in order to be able to account for its effects in damage tolerance evaluation of composite structures. Therefore, this study introduces a novel physical model to isolate and quantify the contribution of fibre bridging to Mode I fatigue delamination. The model distinguishes between monotonic and cyclic components of fibre bridging stress, capturing their individual effects on the strain energy release rate (SERR) in the Paris curve. The monotonic component, based on the Sørensen model, accounts for pre-cracking effects, while the cyclic component is derived by integrating a bridging stress function over the end-opening displacement, with both components modelled by empirical exponential relationships. The model has been validated against established methods such as the Yao model and specific extrapolation techniques, demonstrating improved accuracy in fitting the Paris curve, particularly in accounting for the monotonic influence in the shift of the SERR and the cyclic contribution to the curve slope. Importantly, the model requires only one quasi-static and one fatigue test, reducing the experimental workload. In conclusion, this method provides a more accurate characterisation of fibre bridging effects, making it a robust tool for fatigue delamination analysis.

1. Introduction

Delamination is a damage phenomenon that affects laminated composites and is capable to degrade their structural integrity and reliability [1]. It follows that the accurate prediction and mitigation of delamination are essential in the optimized design of composite structures [2]. Detailed characterisation of delamination, including physical interpretation at the coupon level, can provide reliable parameters for simulating the structural behaviour of composite components and full-scale structures [3,4]. Improved delamination modelling capabilities will allow engineers to predict failure modes and service life with greater accuracy, thereby improving the overall efficiency and safety margins for the design [5].

One key phenomenon affecting Mode I delamination growth is the fibre bridging effect (FB), meaning fibres bridging across the two faces of the delaminated interface spanning the delamination crack plane, which has the main effect of increasing the resistance to the crack growth [6]. This phenomenon introduces additional complexity into the delamination process as bridging fibres can lead to non-linear fracture mechanics behaviour [6]. Various experimental techniques have been employed to gain a better insight into the mechanisms involved in fibre bridging. Yao et al. [7] used in-situ scanning electron microscopy to open the delamination and observe the fracture and bridge formation process. Alternatively, X-ray microtomography has been used to provide an internal view of the fracture aspects and fibre bridges [8–10]. Acoustic emission (AE) has also been used to identify the type of fracture, with signal filters allowing the fracture signals to be distinguished from adhesive/cohesive and fibre breaks, which produce a higher signal [11,12].

Although a proper understanding and quantification of fibre bridging would improve the precision of delamination fatigue growth estimations by refining the current analytical and numerical models [13], measuring the effects of fibre bridging presents significant challenges. Fundamental

* Corresponding author.
E-mail addresses: f.m.monticeli@tudelft.nl, francisco.monticelli@gmail.com (F.M. Monticeli), d.biagini-1@tudelft.nl (D. Biagini), y.mosleh@tudelft.nl (Y. Mosleh), j.a.pascoe@tudelft.nl (J.-A. Pascoe).

https://doi.org/10.1016/j.compositesb.2025.112319
Received 9 December 2024; Received in revised form 7 February 2025; Accepted 18 February 2025
Available online 19 February 2025
1359-8368/

difficulties include accurately quantifying the contribution of bridging during crack propagation and accounting for the variability in fibre-matrix interactions [14,15]. In addition, standard test methods may not fully capture the complexities introduced by fibre bridging [16], requiring the development of advanced experimental techniques and computational models.

Fibre bridging is observed both after quasi-static and cyclic loading application. Under quasi-static loading, bridging fibres cause an increase in the fracture toughness value (G_c), visible in the crack growth resistance curve (R-curve) [17]. In the cyclic regime, the effect of the fibre bridge is similar to quasi-static, increasing the resistance to crack opening and causing a shift in the Paris curve to higher strain energy release rate (SERR) values [18]. As a result, in both cases the fibre bridge creates a higher resistance to propagation compared to what would happen in a theoretical 'clean' crack tip, i.e., without the bridging effect. Given the change in interlaminar fracture behaviour caused by the fibre bridge effect, an important question arises: what is the actual influence of the fibre bridge on fatigue crack propagation? Specifically, how would the crack behave in the absence of the fibre bridge and how would the resulting Paris curve be affected? These questions are particularly relevant because although fibre bridging is usually seen in coupon-scale laboratory tests, it is unclear to what extent it occurs in full-scale structures. To answer these questions, different methods have been used to isolate the fibre-bridging toughening effect.

First, methods have been developed to numerically/analytically quantify the bridging effect. Tian et al. [19] proposed three phenomenological methods (bilinear cohesive zone model, virtual crack closure technique and extended finite element method) and cohesive zone model (CZM) with multi-linear constitutive relation to represent the R-curve and bridging traction effect. The results were validated against experimental data and showed that the multi-linear CZM provides a better fit to the R-curve as it better expresses the constitutive relationships by taking into account the initiation, propagation and bridging stress parameters. Yao et al. [7] applied opening delamination *in situ* in an SEM and used a bilinear cohesive zone formulation through an ABAQUS subroutine to estimate the bridging behaviour. Although in this approach the bridging effect was not modelled, the results emphasised the importance of proper correction of the cohesive law, considering the fibre bridging contribution to the delamination growth.

A physical modelling of the bridging contribution is provided by the bridging laws methods. Fibre bridging provides resistance to opening delamination due to the induced closure stress. Consequently, the effect of fibre bridging is described by bridging laws, which express the relationship between the bridging stress and the crack opening displacement. A bridging law defines how the fibre bridging stress correlates with the crack opening displacement [6,20]. This approach has been widely developed using the J-integral based on phenomenological or analytical approaches. Sørensen et al. [21] applied the bridging law experimentally and captured the resistance to crack propagation as a parameter equal to the strain energy, by integrating the stress through the end-opening of the bridging zone using the J-integral equation. They found no dependence on specimen geometry. Kaute et al. [22] presented a model by analysing the micro-mechanisms contributing to fibre bridge failure, considering only the fibre pull-out mechanism. Later, Sørensen et al. [23] developed a similar micromechanical model to predict the fibre bridging law, considering normal tension for mode I and tangential tension for mode II. A similar approach has also been developed to capture mixed-modes [24], and the effect of a hybrid composite with two types of fibres (carbon and glass) at the delamination interface under cyclic loading [25].

Joosten et al. [26] investigated the interlaminar properties with fibre bridging and demonstrated an overlap between experimental curves and finite element (FE) model predictions under cyclic loading. Their work also highlighted a shift in the Paris curve for larger crack openings due to increased pre-crack length and fibre density. In addition, they observed that mode I is more affected by fibre bridging than mixed mode conditions. Similarly, Dávila et al. [27] performed a numerical analysis of the effect of fibre bridging on the cohesive law with fatigue damage, revealing a shift in the Paris curve when comparing cases with and without fibre bridging. The application of models based on traction-separation behaviour or the bridging law has been implemented for both quasi-static and cyclic loading through cohesive zone FE modelling, demonstrating that fibre bridging plays a crucial role in the observed increase in toughness [28,29].

In contrast, other methods have been developed to remove the bridging effect directly from the Paris curve in a coupon level test. One method was the step sawing of the fibres, which can be used to remove the bridging fibres and estimate the properties of an 'unbridged' crack [30,31]. However, the small crack opening makes cutting the entire fibre bridge region impossible, especially near the crack tip. This forces the use of interpolation to capture the zero-bridging effect. To overcome the interruption and manual removal of fibres, several numerical and analytical models are available in the literature [19,32,33].

Focusing on removing the fibre bridging effect for fatigue curves, Yao et al. [34,35] proposed an empirical model based on the Hartman-Schijve equation to determine the linear region and remove the fibre bridging impact by reducing the values of fracture toughness (G_{IC}) and G_{thr} as a function of crack size. This is performed by assuming the absence of fibre bridging as the crack size approaches zero.

On the other hand, Alderliesten [36] proposed a three-dimensional planar interpolation of the Paris curve and the pre-crack length. The concept is similar to that proposed by Yao, where the reduction to zero pre-crack length removes the effect of fibre bridging. However, both methods require many tests to derive the Paris curves to fibre bridge saturation. The interpolation approach to be adopted is also not uniquely defined in these methods and is open to interpretation. In addition, while the literature addresses the physical aspects of the fibre bridging contribution to the Paris curve, to the best of our knowledge no studies have specifically analysed the monotonic and cyclic contributions of the bridging effect in terms of changes in opening stress and fracture toughness properties, shifting the Paris curve. This gap defines the primary objective of this work.

In order to overcome the aforementioned limitation in the literature, this work aims to present the development, application and validation of an analytical model to characterise the fibre bridge effect in mode I fatigue delamination. As a result, the proposed model aims to explicitly provide the contribution of the monotonic and cyclic components of the fibre bridge phenomenon based on physical aspects. In addition, the proposed methodology can potentially reduce the number of experiments for removing the bridging effect or simulating the fibre bridge saturation on the Paris curve, thus reducing the cost and time of fatigue characterisation.

2. Materials and methods

Pre-impregnated unidirectional (UD) carbon fibre IM7/8552 from Hexcel® was used to produce composite laminates. The laminates were lay-up with 24 layers according to the stacking sequence $[0]_{24}$. Curing was performed in an autoclave using the manufacturer's recommended curing parameters of 120 °C for 2 h and 180 °C for 4 h, with a vacuum of 0.2 bar and a pressure of 7 bar throughout the process.

The specimens were cut on a diamond disc according to the standardised dimensions of ASTM D5528 [37], i.e. 160 x 25 × 3 mm^3, with a PTFE insert to give a length of $a_0 = 50$ mm, measuring from the load application line to the tip of the insert. Aluminium loading blocks with dimensions of 20 x 25 × 10 mm were used to mount the samples to the test rig. Mode I fatigue tests were carried out following ASTM D6115 [38]. A universal servo-hydraulic machine (MTS) with a 500 N load cell was used. The tests were performed under displacement-controlled conditions at a frequency of 2.5 Hz, with a load ratio of 0.1 and constant amplitude. In this study, all parameters influencing crack propagation behaviour - such as frequency, loading ratio, amplitude and lay-up - were carefully controlled and held constant. This approach allowed us to isolate the effect of pre-crack variation, focusing specifically on the characterisation of fibre bridging. The maximum strain energy release rate (G_{max}) was calculated following the compliance calibration (CC) method from ASTM D5528 [37].

The increase in crack size was observed by taking images every 100–1000 cycles and post-processing using the *ImageJ* software. Additionally, the end-opening growth (δ^*) - the opening in the region of the fibre bridge - was measured manually by post-processing the images obtained during the test, ensuring measurement in the region where the fibre bridge is initiated (Fig. 1a), using opening measurement parallel to the load application.

3. Model development

Sørensen et al. [39] developed a relation to measure the fibre bridging stress in mode I intralaminar damage progression in quasi-static loading regime. The formulation follows the *J-integral* relation and considers the equality with strain energy (G_I). The fracture toughness as a material property is generally considered to be constant for homogeneous materials. However, in the context of composites, several damage mechanisms, such as fibre bridging during crack growth, result in a variation in apparent fracture toughness. This variation manifests itself as a non-constant resistance versus crack length, commonly observed in R-curves [40,41]. The difference between the energy at steady-state (G_S) and at the start of propagation (G_0) is directly related to the elastic energy stored in the fibre bridges (Equation (1)). When evaluating different thicknesses, the stiffness of the material increases, and fibre bridge saturation starts to occur at larger crack sizes [39]. However, Sørensen [39] observed that the fibre bridge saturation has the same value of maximum end-opening (δ^*) even when the stiffness of the composite changes due to the different thickness applied, where δ^* is the opening displacement in the region of the fibre bridge zone (Fig. 1a). The fibres begin to break when the critical opening displacement is reached [23], which makes the approach more wider for different configurations of composite materials. At the same time, new fibre bridges are formed at the crack tip and the length of the bridge region stays constant, as the bridging region moves forward with the growth of the delamination [21]. Therefore, the integral across the end-opening of the fibre bridging stresses equals to the difference between the initiation and saturation of strain energy (G) of the R-curve [21,39,42].

$$G_r = G_0 + \int_0^{\delta^*} \sigma(\delta^*)d\delta^*, \sigma(\delta^*) = \frac{\partial G_r}{\partial \delta^*} \tag{1}$$

where, G_r is the fracture toughness, G_0 is the energy release rate at the crack tip (zero-bridging), δ^* is the end-opening in the fibre bridging opening, δ^*_{sat} is the end-opening at saturation of the fibre bridging level (which changes G_r by G_s), and $\sigma(\delta^*)$ is the fibre bridging stress at the given end-opening.

From the fitting of the R-curve based on end-opening (G_r–δ^*), Sørensen et al. [39] defined Equation (2) to model the growth of relative fracture toughness considering the bridging law in the quasi-static regime. By combining Equation (1) and Equation (2) and considering that G_0 and ΔG_s (strain energy at saturation region minus G_0) are constant with respect to δ^*, we obtain equation (3). As the R-curve reaches its steady state value G_S when δ^* is equal to δ^*_{sat} ($\delta^*_{min} < \delta^* < \delta^*_{sat}$), the bridging zone maintains a constant length and a self-similar opening profile [39]. Based on this, the fibre bridging stress is given by Equation (3) and results in the fibre bridging stress along the end-opening, which represents the bridging stress along the fibre bridging zone (Fig. 2b).

$$G_r = G_0 + \Delta G_s \left(\frac{\delta^*}{\delta^*_{sat}}\right)^{1/2} \tag{2}$$

$$\sigma(\delta^*) = \frac{\Delta G_s}{2\sqrt{\delta^* \bullet \delta^*_{sat}}}, for\ \delta^* > \delta^*_{min} \tag{3}$$

Where, σ is the fibre bridging stress, δ^* is the end-opening at the bridging zone, ΔG_s is the difference between minimal and maximal strain energy in the R-curve $\Delta G_s = G_s - G_0$, and G_S is the strain energy at the saturated fibre bridging region (steady-state region).

Equation (3) provides a stress tending to infinity for zero opening and does not explicitly impose a limit on the maximum end-opening. To overcome these limitations, the following boundary conditions were applied: *i)* a linear interpolation was used between the maximum and zero stress to simplify the representation of bridging formation, from zero-bridging to the onset, $\sigma(\delta^*) = m \bullet \delta^*$, for $\delta^* < \delta^*_{min}$, where $m =$

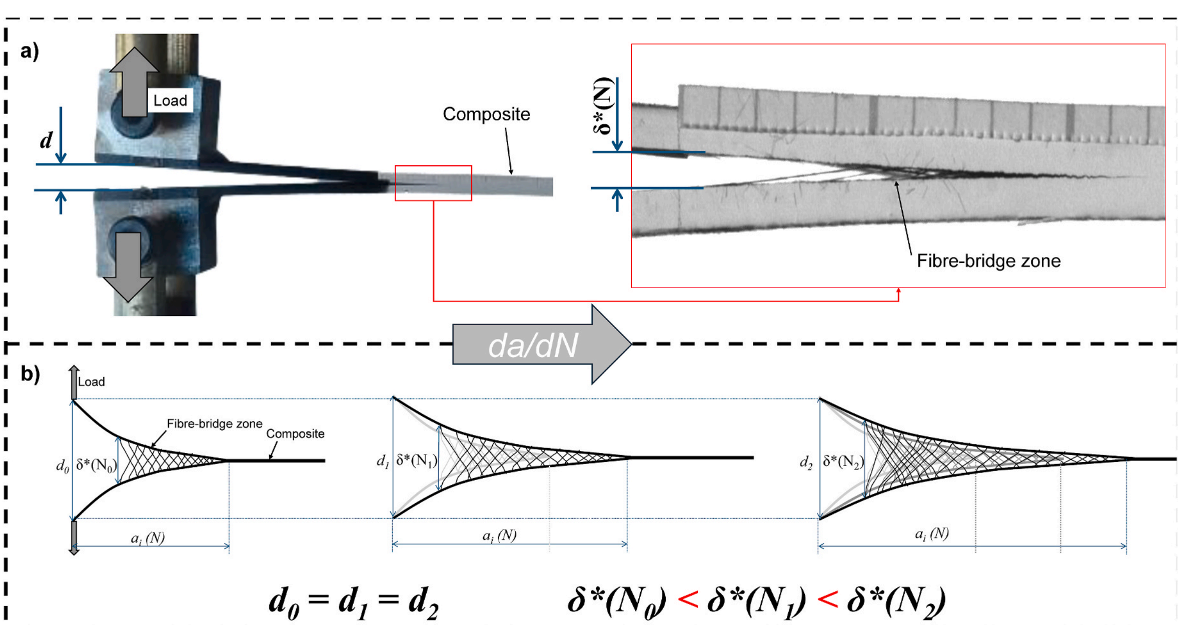

Fig. 1. a) Definition of open delamination δ (load region) and end-opening δ* (fibre bridging region), and b) illustration of incremental end-opening during fatigue delamination as a function of compliance change.

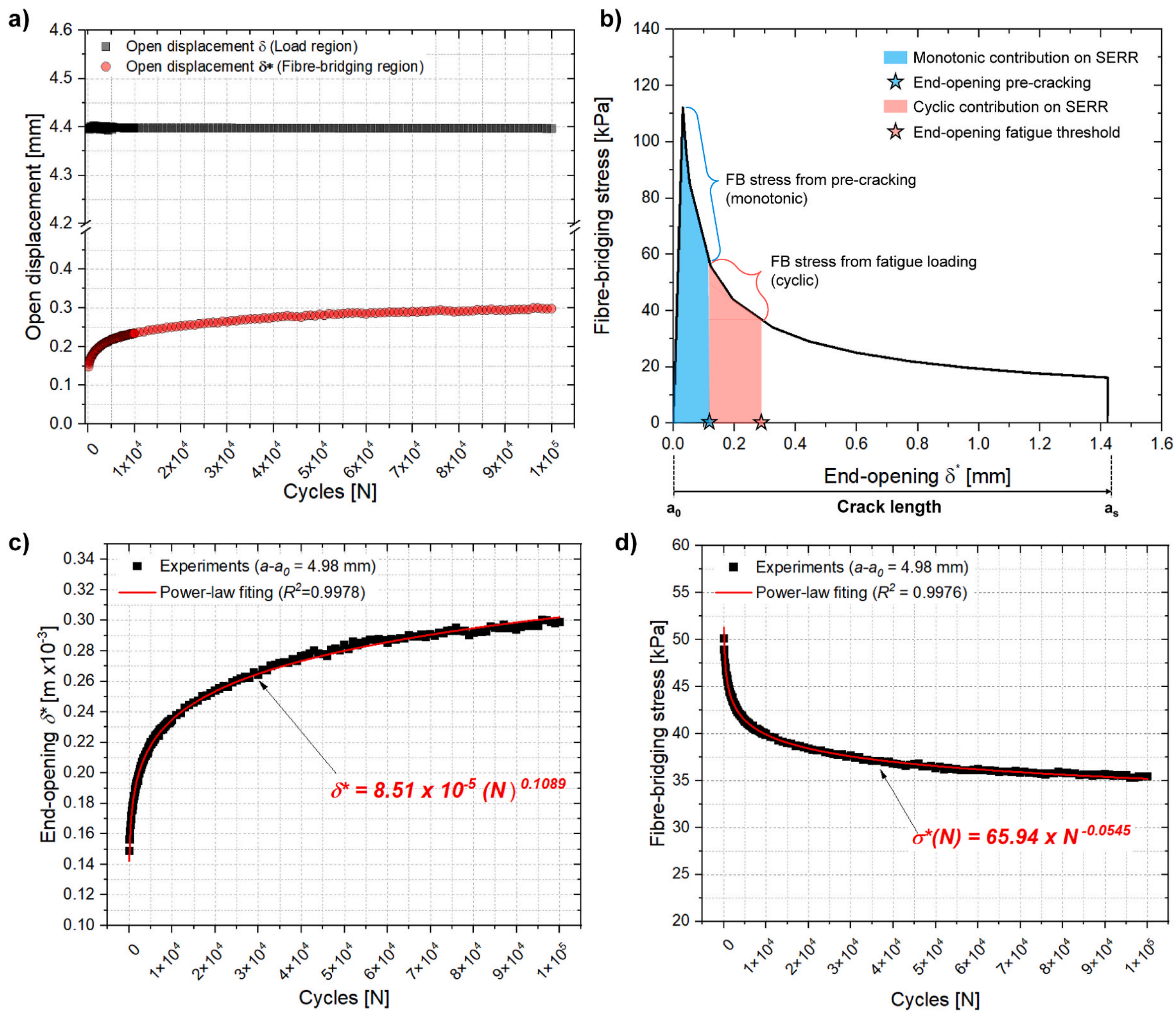

Fig. 2. Illustration of: a) open displacement (*d*) at the load region and end-opening (δ*) at fibre bridging region; b) fibre bridging stress from the quasi-static test and illustration of bridging in pre-cracking and fatigue loading through fibre bridging stress curve, c) end-opening (δ*) along the cycles, and d) Fibre bridging stress along the cycles.

$\sigma(\delta^*_{min})/\delta^*_{min}$; and *ii)* The stress is set to drop to zero after the maximum end-opening (δ^*_{sat}) to ensure that no additional energy is introduced beyond the point of fibre bridge saturation, $\sigma(\delta^*) = 0$, for $\delta^* > \delta^*_{sat}$.

This formulation of the bridging stress was previously developed for the quasi-static regime but could also be used to explain the shift of the Paris curve at higher strain energy values due to the increase in fibre bridge stress. On the other hand, a shift in the Paris curve towards lower SERR values can be obtained if the energy associated with the fibre bridge stress is removed. This would provide the zero-bridge curve reflecting the inherent fracture toughness without fibre bridge effects [43]. According to Yao et al. [34], the R-curve in fatigue is not the same as in quasi-static loading. This highlights the importance of not using a simplified normalisation of the similitude parameter in Paris equation (G_{max}/G_{IC}, taking G_{IC} from QS), as the cyclic contribution generates an important contribution to the fibre bridge densification. However, the fibre bridging stress curve remains unchanged because the stress transfer mechanisms governing fibre bridging are primarily determined by the fibre-matrix interaction and the intrinsic properties of the fibre.

Starting from this, the first consideration is that the end-opening is not constant during the fatigue regime, and thus becomes a function of cycle: $\delta^*(N)$. This behaviour was experimentally observed in this work during crack growth under cyclic loading. There is a change in compliance due to the crack propagation, and consequently in the end-opening region. The compliance changes the beam bending and increases the end-opening along the cycles $\delta^*(N_0) < \delta^*(N_1) < \delta^*(N_2)$, which has the effect of increasing the fibre bridge density and the corresponding stress (Fig. 1b) – even considering that displacement control was used during cyclic loading (i.e. $d_{max} = d_0 = d_1 = d_2$). The end-opening increment as a function of cycle number can be modelled by the power law in Equation (4), in which the initial end-opening δ^*_{QS} is defined during the pre-crack testing, following the standard.

$$\delta^*(N) = \delta^*_{QS} \bullet N^{m_1} \tag{4}$$

where, δ^*_{QS} is the initial end-opening at the quasi-static level of the pre-cracking definition, N is the number of cycles, and m_1 is a fitting constant.

Based on this principle, there is then an additional dependency of the fibre bridge stress as a function of cycles $\sigma^*(N)$ to be included in the model. The fibre bridge (FB) stress is modelled with the Basquin-law [44], Equation (5). It is assumed that the gradual increase of (δ^*) values as well as the progressive reduction in bridging stresses can be interpolated via an exponential relationship.

$$\sigma^*(N) = \sigma^*_{QS} \bullet N^{m_2} \tag{5}$$

where, $\sigma^*(N)$ is the FB stress $\sigma^*(\delta^*)$ as a function of number of cycles, σ^*_{QS} is the initial stress (from the quasi-static relation) and m_2 is a fitting constant.

Fig. 2a shows the results of the displacement (d) controlled fatigue loading in the loading region, indicating that end-opening increase is governed by the crack growth relation and the change in bending of the beam (illustrated in Fig. 1b). This change of end-opening is related to the generation of bridging fibres. During a quasi-static test, the influence of fibre bridging can be observed by the change in G_r (R-curve). In a fatigue test, it can also be observed by the shift of the Paris curve to higher SERR values as longer pre-crack lengths are used [45–47], but also by the change in compliance of the beam during the fatigue delamination growth, increasing the fibre bridging density and, consequently, providing an increment on the stress resisting to the crack opening. Fig. 2b provides the stress of bridging at the quasi-static level, calculated from Equation (3), which represents the stress distribution along the bridging region, and the area under the graph is associated with the crack growth resistance energy. The initial linear region represents the part of the curve where the fibre bridge begins to form and adds contribution to the crack opening resistance, with the maximum stress occurring at the minimum opening value. Whilst extending the curve to zero end-opening would theoretically lead to infinity, there is a finite region at the crack tip where starts the bridge formation. Fibre bridging occurs progressively within the damage zone rather than instantaneously, avoiding singularities in the stress distribution. In addition, an infinite bridging stress is not physically possible as the material has a finite strength and the fibre bridging mechanism is inherently limited by the mechanical properties of the fibres and matrix [48]. To overcome that, a linear fit was applied (following boundary condition *i, defined above*) between the maximum stress and zero to represent the growth of the fibre bridge from zero to its onset [7,19,49].

The fibre bridge zone moves with the crack propagation and the energy under the stress curves remains constant throughout the propagation, keeping the G_r curve constant at bridge saturation. The fibre bridging stress curve region grows from the initial quasi-static contribution (blue region and the FB stress – Fig. 2b). Applying the cyclic loading under displacement control, crack propagation causes a change in the compliance of the material, increasing the end-opening values and shifting the stress curve forward (red region under FB stress – Fig. 2b).

Considering the crack propagation and the increasing end-opening (δ^*) values during cyclic loading, the power law-based Equation (5) is applied for a specimen with a–a_0 = 4.98 mm. δ^* is measured in the region shown in Fig. 1a. Additionally, Fig. 2d shows the fibre bridge stress relation over the cycles of the same specimen, i.e., a–a_0 = 4.98 mm, considering a displacement-controlled fatigue test. The curve in Fig. 2d is calculated for each group of cycles using Equation (3), applying the end-opening values based on the cycle-dependent function, as shown in Fig. 2c. The end-opening (δ^*) changes over the cycles, following the variation of the bending of the specimen arms as the delamination extended. This indicates an increase of bridging area until the crack stopped growing; the crack arrest being a consequence of the test being conducted under displacement control.

The choice of the power law to model the end-opening displacement and fibre bridging stress evolution over cycles is based on the observed behaviour of the experimental data (Fig. 2). In particular, the growth of end-opening values is influenced by the compliance associated with crack growth, resulting in an exponential-like relationship. The power law provides a good fit for both cases ($R^2 > 0.99$). Although this approach simplifies some of the variability observed in the experiments, it effectively captures the overall exponential behaviour of the data. The power law function combines simplicity and representativeness. Once the FB stress function is plotted as a function of the number of cycles, the model can be adapted to ensure measurement of the strain energy associated with crack growth during cyclic loading.

Considering that the pre-cracking produces an initial bridging stress and the propagation during the fatigue provides a fluctuation of stress over cycles, the energy associated with crack growth resistance from fibre bridging can be divided into a monotonic (Equation (6)) and cyclic (Equation (7)) component. Equation (6) is the result of the monotonic contribution considering the end-opening $\delta^* > \delta^*_{min}$ which is summed to the first part of fibre bridge formation adding the equation $\sigma(\delta^*) = \left[\sigma(\delta^*_{min})/\delta^*_{min}\right] \bullet \delta^*$, for $\delta^* < \delta^*_{min}$. Both equations represents a constant value throughout the fatigue test.

$$(G_{FBZ})_{monotonic} = \int_{\delta^*_{min}}^{\delta^*_{QS}} \sigma(\delta^*)d\delta^*, for\ \delta^* > \delta^*_{min} \tag{6}$$

Equation (7) shows the crack growth resistance (associated with SERR) as a function of the number of cycles. There is a difference between the end-opening from the quasi-static test δ^*_{QS} and from fatigue test $\delta^*(N)$ – related to the cycle number. By isolating the common parameter (cycles N) of Equation (4), we developed Equation (8). In the case of the initial end-opening application, the values of σ_{QS} are the initial stress value of the fibre bridge and δ^*_{QS} is the end-opening generated according to each pre-crack length. Applying Equation (8) to Equation (5), replacing the new values of N, we obtain Equation (9) which can be simplified into Equation (10).

$$(G_{FBZ})_{cyclic} = \int_{\delta^*_{QS}}^{\delta^*(N)} \sigma(\delta^*, N)d\delta^* \tag{7}$$

$$N = \left(\frac{\delta^*(N)}{\delta^*_0}\right)^{1/m_1} \tag{8}$$

$$\sigma(\delta^*) = \sigma_{QS}\left[\left(\frac{\delta^*(N)}{\delta^*_{QS}}\right)^{1/m_1}\right]^{m_2} \tag{9}$$

$$\sigma(\delta^*) = \sigma_{QS} \bullet \delta^*_{QS}{}^{(-m_2/m_1)} \bullet [\delta^*(N)]^{(m_2/m_1)} \tag{10}$$

where, δ^*_{QS} represents the end-opening for pre-crack formation (quasi-static) and the $\delta^*(N)$ is the values represent the end-opening for cycle (N).

By collecting the constant parameters in the form of $k = \sigma_{QS} \bullet \delta^*_{QS}{}^{(-m_2/m_1)}$ we can compress Equation (7) into Equation (11). The integral solution is given in Equation (12). After streamlining the integral and again expanding k, Equation (13) is obtained, representing the empirical model of the cyclic contribution of the fibre bridge to the strain energy values $(G_{FBZ})_{cyclic}$.

$$(G_{FBZ})_{cyclic} = \int_{\delta^*_{QS}}^{\delta^*(N)} k \bullet \delta^{*(m_2/m_1)} d\delta^* \tag{11}$$

$$(G_{FBZ})_{cyclic} = k\left[\frac{(\delta^*)^{((m_2/m_1)+1)}}{\frac{m_2}{m_1}+1}\right]_{\delta^*_{QS}}^{\delta^*_{Nmax}} \tag{12}$$

$$(G_{FBZ})_{cyclic} = \frac{\sigma_{QS} \bullet \delta^*_{QS}{}^{(-m_2/m_1)}}{\frac{m_2}{m_1}+1}\left\{[\delta^*(N)]^{\left(\frac{m_2}{m_1}+1\right)} - \left[\left(\delta^*_{QS}\right)^{\left(\frac{m_2}{m_1}+1\right)}\right]\right\} \tag{13}$$

The constants m_1 and m_2 were calculated by exponential fitting Equations (4) and (5) using OriginLab® software. The model shows that a relationship of $m_2 = -0.5m_1$ governs, taking into account an energy balance condition and an empirical dependence of the system on the relationship between the slope of end-opening growth $\delta^*(N)$ and the resulting stress $\sigma^*(N)$. This statement can be validated by comparing the slopes in Fig. 2d (corresponding to m_2) and Fig. 2c (corresponding to m_1), where the ratio $m_2/m_1 = -0.5$ (– 0.0545/0.1089). Equation (13) can therefore be simplified to Equation (14). Finally, the contribution of the fibre bridge to the total SERR values is represented by the sum of the monotonic and cyclic contributions based on superposition principle

(Equation (15)).

$$(G_{FBZ})_{cyclic} = \left(2\sigma_{Qs} \bullet \sqrt{\delta^*_{QS}}\right)\left(\sqrt{\delta^*(N)} - \sqrt{\delta^*_{QS}}\right) \tag{14}$$

$$(G_{FBZ})_{total} = (G_{FBZ})_{monotonic} + (G_{FBZ})_{cyclic} \tag{15}$$

where, $G_{FBZ,i}$ represents the strain energy related to the fibre bridging zone for initial quasi-static monotonic loading and for cyclic loading.

The use of the superposition principle (Eq. (15)) in the proposed model is justified by the need to distinguish and quantify the monotonic and cyclic contributions of the energy stored in the fibre bridge zone, which provides resistance to crack propagation. As can be seen in the literature [31,43], the increase of the pre-crack length produces a densification of fibre bridging, which causes the shift of the curve towards higher SERR values, keeping the slope of the curves very close to each other. This principle is applicable because the monotonic and cyclic components are associated with different physical phenomena that occur at different stages during the fatigue test:

- **Monotonic component $(G_{FBZ})_{mono}$:** Represents the energy storage during pre-crack initiation under quasi-static loading. It can be considered constant throughout the test as it provides the initial increase in strain energy from which the crack then develops further during cyclic loading. This contribution is therefore directly related to the initial resistance of the fibre bridge zone before the cyclic variation.
- **Cyclic component $(G_{FBZ})_{cyclic}$:** It is associated with the incremental change in end-opening (δ^*) and fibre bridge density during cyclic loading due to the change in compliance during crack growth. The cyclic energy is modelled as a function of the number of cycles and reflects the progressive behaviour of saturation and stress redistribution in the fibre bridge zone.

The mathematical model developed is based on the separation of these contributions. The sum of these components (Eq. (15)) allows the description of the global behaviour of the crack propagation resistance $(G_{FBZ})_{total}$, respecting the boundary conditions and the physical phenomena observed experimentally. The fit of the experimental data to the model (which will be shown below) confirms the validity of the approach, while the application of the superposition principle simplifies the interpretation of the results, and the quantification of the energy associated with the fibre bridging zone.

Furthermore, the superposition principle is consistent with the J-integral based formulation, which considers the total energy as the sum of local contributions associated with different regions of the crack. This approach allows, for example, the derivation of adjusted Paris curves (with and without the effect of fibre bridges). In other words, it is possible to subtract the fibre bridge stress directly from the experimental G_{max} values to generate the zero-bridging Paris curve. Similarly, this work proposes to add the fibre bridge stress to estimate the Paris curve with fibre bridge saturation. This reduces the number of experiments required for such characterisation.

Fig. 3a shows the evolution of the crack-opening resistance due to

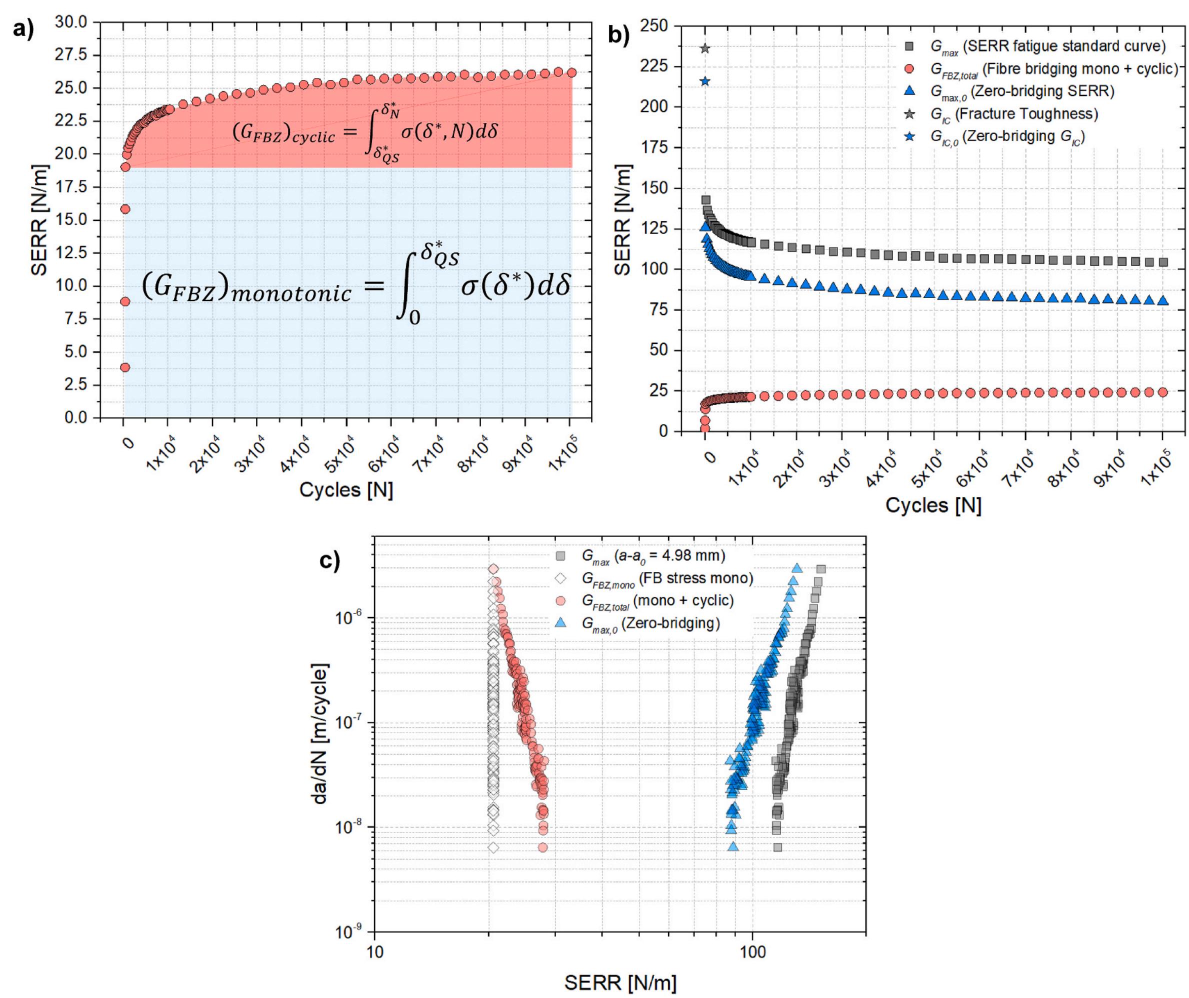

Fig. 3. a) Illustration of monotonic and cyclic strain energy, b) SERR versus cycles, and c) effect of fibre bridging in Paris curve.

fibre bridging. The lower part of the curve (blue region) is associated with the monotonic resistance energy that comes from quasi-static pre-cracking developed prior to the fatigue test to determine the values of a–a_0. The result above the monotonic region represents the non-constant cyclic contribution. The trend of the cycle-varying contribution to SERR is monotonically growing as fibre bridge density increases during the cycles.

By considering the energy associated with bridging that has just been derived, it is possible, for instance, to remove the bridging effect of the experimental SERR *G-N* curve. In Fig. 3b, the G_{max} curve (black square – standard measurement of SERR) shows the experimental behaviour of the strain energy decay over the cycles as the test is performed with displacement control [50]. This curve is for the sample with a pre-crack (a–a_0) = 4.98 mm, which provides an initial bridging formation associated with a monotonic contribution of fibre bridging stress that can be associated with resistance to crack growth ($G_{FBZ,mono}$). This fibre density increases during the cycle propagation in a less extensive way than the monotonic part, giving the strain energy growth curve during the cycles ($G_{FBZ,cyclic}$) according to Equation (14). The sum of both parameters represents the superposition principle model (Eq. (15)). The red circles in Fig. 3b are the same curve as in Fig. 3a, and both represent the ($G_{FBZ,total}$). Subtracting ($G_{FBZ,total}$) from G_{max} results in the removal of the energy storage associated with the fibre bridging stresses, giving the intrinsic SERR curve without the effect of bridging $G_{max,0}$ (blue triangles – zero-bridging SERR).

Applying the same analysis to the Paris curve (Fig. 3c), we observe the experimental curve G_{max} (a–a_0 = 4.98 mm), which generates the Paris constants according to the relation in Equation (16) [51]. Applying Equation (6), we have the $G_{FBZ,mono}$ curve, which represents the constant resistance to the crack growth associated fibre bridge formation for the 4.98 mm pre-crack. In other words, the monotonic part is responsible for the shift in the curve at higher values, as the $\mathrm{G_{FBZmono}}$ values are constant throughout the *da/dN* curve.

By adding the effect of the change in beam compliance in the fibre bridging region due to cyclic loading, the impact of the bridge becomes variable and increases with crack growth, as observed in the $G_{FBZ,total}$ curve shown in Fig. 3c, which considers the monotonic + cyclic contribution. This function is obtained by Equation (15), where the monotonic contribution (Eq. (6)) is added to the cyclic contribution (Eq. (14)) to give the total strain energy value associated with the fibre bridge stress. By subtracting the $G_{FBZtotal}$ curve from the experimentally measured curve (labelled $\mathrm{G_{max}}$ in Fig. 3c), we obtain the zero bridging curve, labelled $G_{max,0}$ in Fig. 3c. As the monotonic bridging remains constant, while the cyclic bridging contribution increases towards longer crack lengths (corresponding to lower da/dN for displacement control), the slope of the $G_{max,0}$ curve is shifted compared to the G_{max} curve.

Equation (17) shows the relationship between the Paris curve (Eq. (16)), which could provide the zero-bridging effect (intrinsic SERR) by removing the energy storage from FB stress or adding the saturation of the bridging effect for different pre-crack lengths (estimation of the Paris curve with bridge saturation). Therefore, from the generic model, it is possible to remove the effect of the fibre bridge or to estimate the fibre bridge saturation of the Paris curve using at least a single static test to provide the bridging stress curve and a fatigue test as a reference curve, as shown in Fig. 3c through the $G_{max,0}$ (zero-bridging) curve.

$$\frac{da}{dN} = \alpha\left(G_{max,i}\right)^{\beta} \tag{16}$$

$$\frac{da}{dN} = \alpha\left(G_{max,0}\right)^{\beta} = \alpha\left(G_{max,i} \pm G_{FBZ,total}\right)^{\beta} \tag{17}$$

where, α and β represent Paris constants, and i represents the different crack length index (i.e., $i = a - a_0$).

While it is true that the Paris equation is a phenomenological model rather than a fundamental law, it can still be used to make accurate predictions when supplied with appropriate experimental data to calibrate the models, which provides a feasible engineering approach in structural design [43,51,52]. To avoid unconservative crack growth predictions, it is important to be able to correct for the effect of fibre bridging during material characterisation experiments, as fibre bridging may not occur in operational structures. On the other hand, if it can be assured that fibre bridging *will* occur, then if designers wish to exploit the toughening effect of the bridging, they need a tool that enables quantification of this effect on crack growth. Therefore, the proposed model focuses on clarifying the relationship between the physical mechanisms of fibre bridging driving delamination growth and the resulting macroscopic behaviour (G_{max}), demonstrating its practical utility.

4. Model application

4.1. Model application to quasi-static regime

In order to apply the fatigue modelling of the bridging effect, it is first necessary to perform mode I delamination under a quasi-static regime to develop the stress curve of the fibre bridge, capturing the saturation of the fibre bridge in terms of crack size and end-opening displacement (δ^*). Fig. 4a shows the results of the R-curve where the propagation relation (a–a_0) and fracture toughness values are established. It is possible to observe the increase in G_I values at the start of propagation until the steady state is reached, i.e., G_S – fracture toughness at saturated FB. The determination of fibre bridge saturation, as reflected in the R-curve, can vary from specimen to specimen as it is not a trivial task to determine the exact moment when saturation begins. To ensure consistency, we have defined crack growth saturation (a_s) by combining both the R-curve and visual analysis of the specimen, as shown in Fig. 1a.

The application of Equation (2) gives propagation resistances in the initial propagation region and G_S; an increase in strain energy is associated with fibre bridge development. Fig. 4b shows the G_r curve as a function of the opening in the fibre bridge region (end-opening δ^*), with the points representing the experiments and the curves in the solid and dashed lines fitting Equation (2). To ensure higher reliability of the results and to account for material variability, three curves were generated, one from the average of the experimental results (solid lines) and one each from the minimum and maximum regions of the experimental points (dashed lines). The three curves represent the relative increase in crack opening resistance work due to the presence of the fibre bridge over the entire experimental range.

Following Equation (3), it is possible to generate the curve representing the stress distribution of the fibre bridge between the start of propagation and the steady state region (Fig. 4c). This curve is plotted as a function of the end-opening. After reaching the maximum end-opening, the values drop to zero as the fibres break at the critical opening. The maximum stress values σ_0 are 112.25, 132.82 and 101.51 kPa for the average, maximum and minimum curves, respectively. The maximum end-opening values were $\delta^*_{sat} = 1.42$ mm for all cases. δ^*_{sat} represents the maximum fibre elongation before rupture, which is determined by the tensile strength of the fibre. Any value above this threshold will inevitably lead to fibre breakage, as confirmed by experimental observations in both quasi-static and fatigue tests. The relation between the stress and resistance curves of the fibre bridge is given by Equation (6), where the integral of the curve in Fig. 4c provides the work of stress resistance associated with the G values in Fig. 4b [39,53].

4.2. Model application to fatigue regime

Fatigue tests were carried out with different initial pre-crack values. A larger pre-crack size favours an increase in the density of fibre bridges

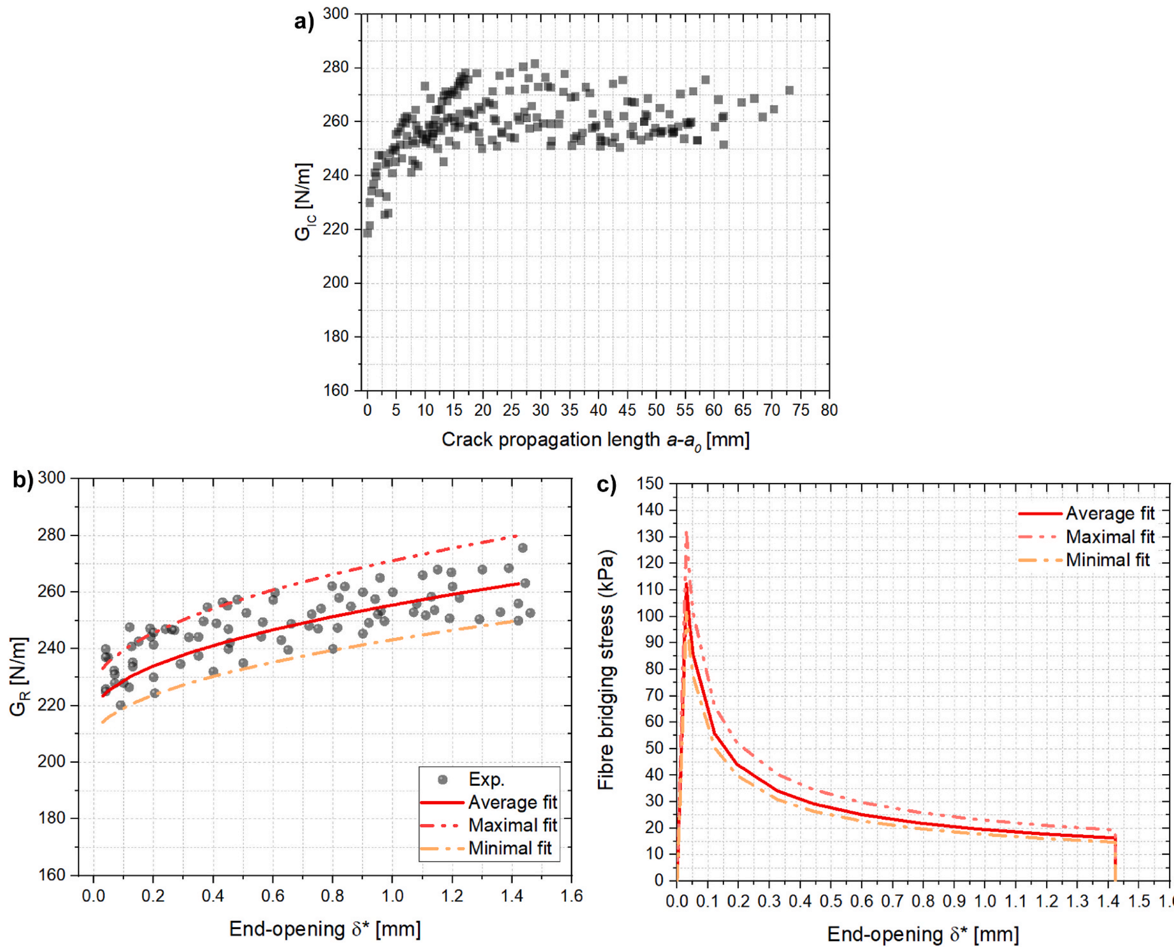

Fig. 4. Quasi-static results: a) R-curve, b) The crack growth resistance as a function of end-opening, and c) e local bridging stress as a function of the local crack end-opening.

and causes a shift in the Paris curve to higher values of G_{max} experimental. This happens since the higher density of the fibre bridge increases the resistance to mode I delamination which now requires more energy to propagate [31,43]. Similar to the literature, the experimental curves of mode I fatigue crack propagation can be observed in Fig. 5. The dots represent the experimental results, and the line are the Paris fitting (Eq. (16)). In this figure, all curves include the effect of crack tip propagation in addition to the resistance created by the fibre bridge, which is directly associated with a distinct pre-crack length, i.e., 2.35–31.80 mm.

The application of the proposed model (Equation (17) - reducing bridging effect) to each curve in Fig. 5 yields the intrinsic Paris curves without the influence of bridging effects, as shown in Fig. 6. The dots represent the prediction curves based on zero-bridging, using Eq. (17),

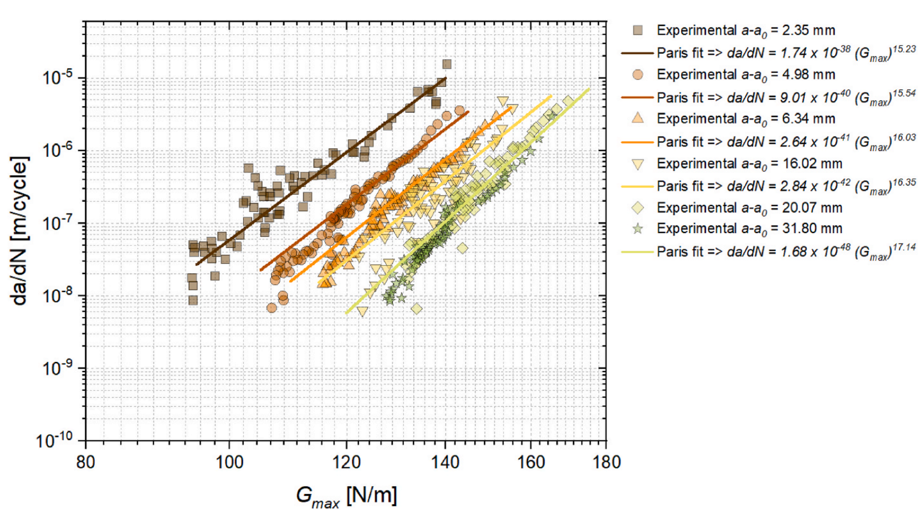

Fig. 5. Experimental Paris curve relation with different initial crack lengths (a–a_0).

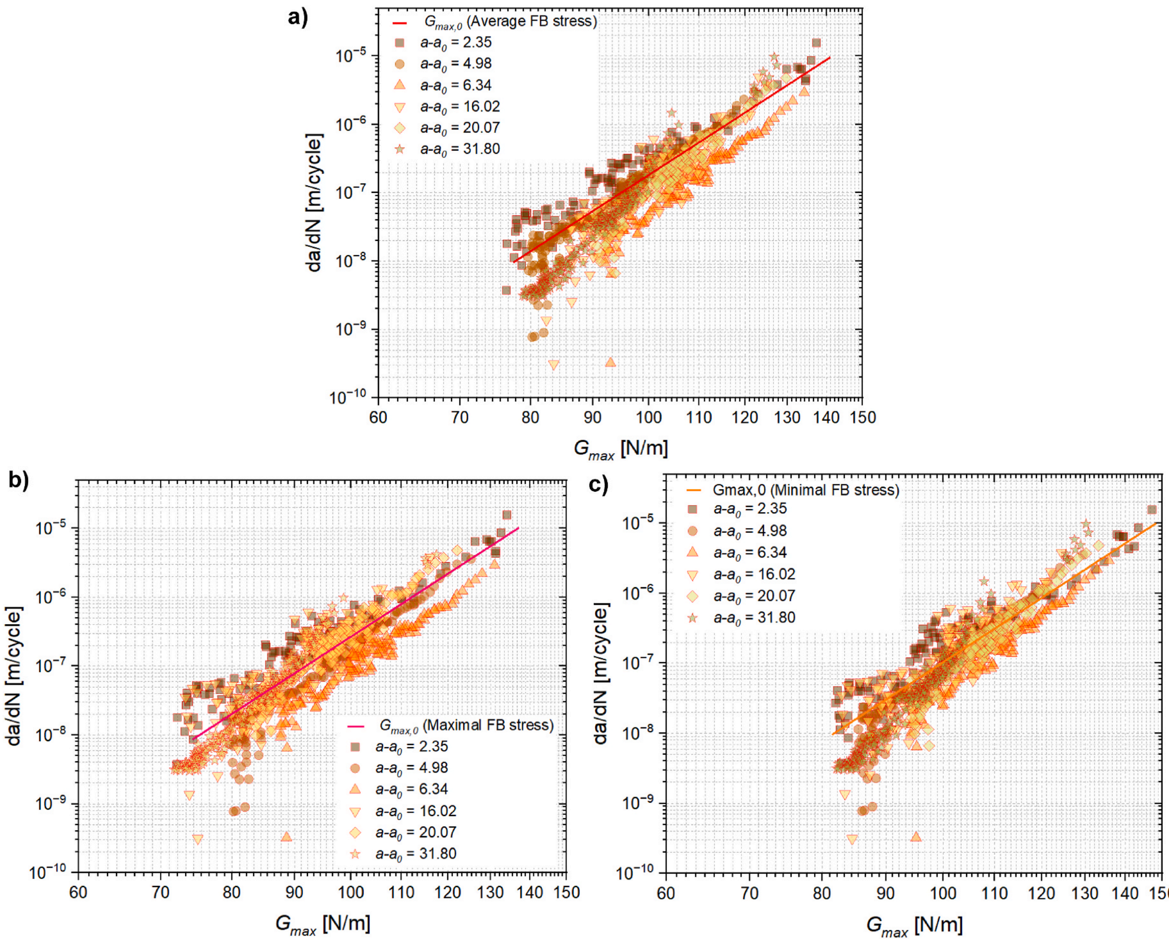

Fig. 6. Predicted zero-bridging Paris curve for: a) average FB stress b) maximal FB stress and c) minimal FB stress.

and the lines represents the Paris fitting. This reduction has been made considering the maximum, minimum and average distribution of the fibre bridging stress, as illustrated in Fig. 4c, following the description in Section 3. In this way, the approach provides a good fit, considering that all predicted curves with different pre-crack lengths fit in the same range for each case of calculated bridging stress, i.e. average (Fig. 6a), maximum (Fig. 6b) and minimum FB stress (Fig. 6c). The variability of the experimental points remains when using the proposed model, as can be seen in each curve.

The monotonic contribution is fatigue independent, as it results from the removal of the fibre bridging stress during pre-crack formation, which is constant at the start of the test. This constant bridging effect is excluded from the similitude parameter G_{max} in the Paris equation, leading to a pronounced change in the constant alpha (α). On the other hand, there is an increase in the contribution of the FB stress as a function of the number of cycles as the end-opening increases during fatigue propagation, which we denote as the cyclic component of the bridging effect. In this way, the total integration of the stresses in both the mono and cyclic tests gives $G_{FBZ,total}$ (mono + cyclic) and promotes the reduction of the strain energy region and thus also changes the slope of the Paris curve, which represents the zero-bridging Paris curve ($G_{max,0}$ zero-bridging).

Fig. 7a shows the removal of the FB stress on the Paris curve compared to experimental curves with different pre-crack lengths. The caption identifies the experimental, the Paris fitting and the simulated data (predicted based on the proposed model). From the experimental data, it is possible to fit the new Paris parameters (α and β). The reduction in the slope of the curve (β) was ≈34 %, changing from a range of 15.23–17.14 (depending on the value of a–a_0) to the range of 10.53–10.84. Similarly, a shift in the curve towards lower SERR values can be observed as the stress generated by the fibre bridge is removed.

The range of possible fibre bridge stress values based on the variability in the quasi-static curve (Fig. 4c) can be analysed based on min, max and average FB stress curves. In Fig. 7a, the minimum FB stress was not able to guarantee the complete removal of the fibre bridge effect, since the region of the intrinsic $G_{max,0}$ (zero-bridging - minimum FB stress) is in the same region as the one with the lowest fibre bridge density in the experimental data (a–a_0 = 2.35 mm). This suggests that the minimum FB stress based on the model shown in Fig. 4c underestimates the actual fibre-bridging stress. The new value of SERR with zero-bridging ($G_{max,0}$ zero-bridging) based on the average and maximum effect of the FB stress show the biggest reduction, suggesting an appropriate removal of the bridging effect.

The change in slope and decrease in SERR values for a given *da/dN* compared to the standard Paris curve are the main parameters affected by excluding the bridging effect (Fig. 7a). After the fibre bridging effect is removed, the intrinsic SERR shown is dissipated only at the crack tip, essentially by adhesive and cohesive failure. This damage mechanism favours the toughness behaviour, compared to the curves that have the bridging effect, evidenced by a decrease in the slope of the Paris curve.

It can therefore be empirically concluded that the removal of the monotonic FB stress is mainly responsible for the reduction in opening stress (shift to lower SERR). When the cyclic contribution is added, the change in slope of the Paris curve is more pronounced, associated with more fibre bridge formation in the final cycles (long crack length) than in the early cycles. The range between $G_{max,0}$ (zero-bridging), based on either the maximum or the average FB stress, is recommended to ensure a more conservative analysis of what can be considered in terms of

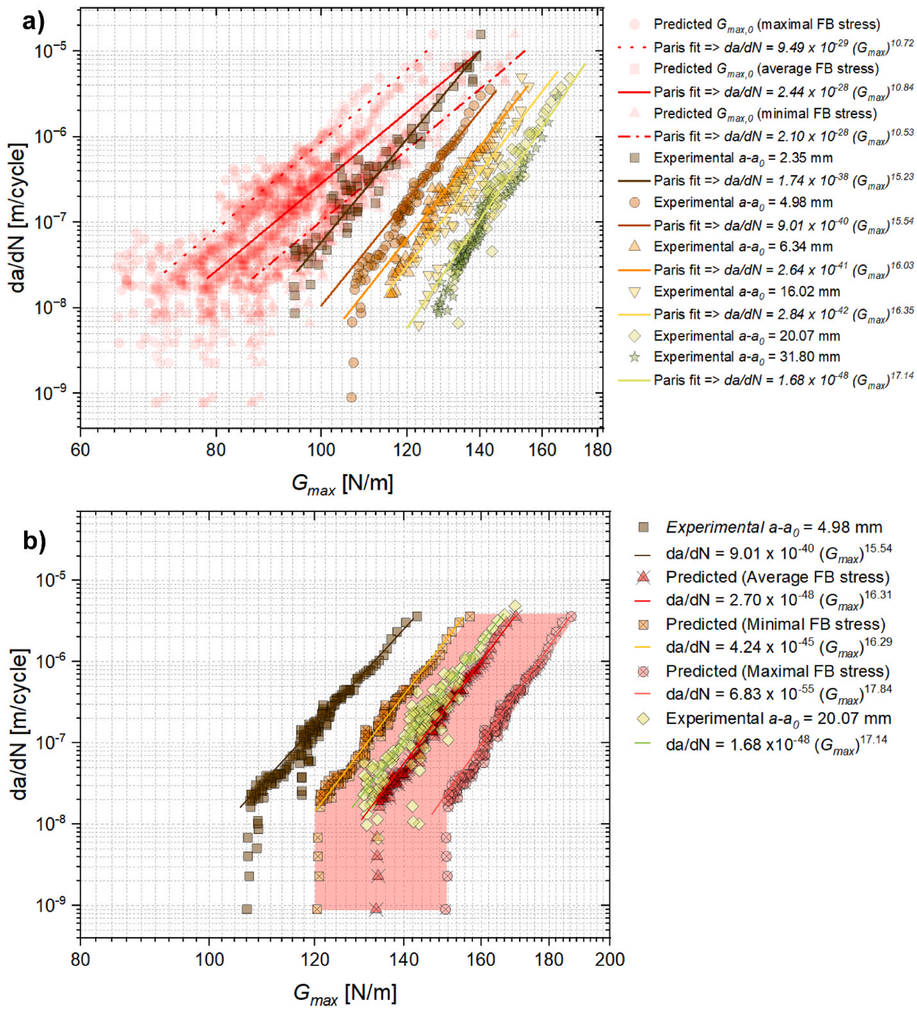

Fig. 7. Paris curve: a) zero-bridging modelling and b) prediction fibre bridging saturation.

complete removal of the fibre bridging effect.

The limitation of the model is the challenge of measuring the crack opening in the fibre bridging zone, considering a region of small opening (smaller than the loading region). To achieve this, it is necessary to use methods with a measuring range of 0.03–1.42 mm, guaranteeing a sensitivity of 10 μm. Errors in interpreting visual measurements from image processing lead to a greater deviation in the Paris curves (Fig. 6).

Equation (17) can be adjusted to add, rather than remove, the fibre bridge effect from an initial curve, giving Equation (18), where, i represents the average, maximal or minimal stress of FB,

$$\frac{da}{dN}=\alpha_i\left[(G_{max})_{exp}+\left(\int_0^{\delta^*_{sat}}\sigma(\delta^*)d\delta^*\right)_{total\,FB\,stress}-\left(\int_0^{\delta^*_{QS}}\sigma(\delta^*)d\delta^*\right)_{Pre-crack}\right]^{\beta_i} \tag{18}$$

With Equation (18), it is possible to predict the fibre bridge saturation behaviour in the Paris curve without performing the full test (Fig. 7b). Equation (18) represents the experimental G_{max} values added to the entire integral of the fibre bridge stress curve (Fig. 4c). It is important to remove the fibre bridge stress already present in the experimental G_{max} curve so that the value associated with the FB stress from pre-crack formation is not doubled. The experimental curve a–a_0 = 4.98 mm was used as a reference curve to simulate the Paris curve at fibre bridge saturation and compared with the experimental results in the saturation region a–a_0 = 20.07 mm. The prediction curves were developed by taking into account the range of maximum, minimum, and average stress effects on the fibre bridge. In this case, it can be observed that the predicted curve based on the average FB stress values overlaps the experimental value, providing a better fit.

The variability between the proposed prediction model and the experimental data (a–a_0 = 4.98 mm) showed an average error of 4.62 % in curve slope (β) for the model considering maximum, average and minimum fibre bridge stress. On the other hand, it is possible to observe a greater variability in the estimated SERR region (red area), where the error between the simulated and experimental model was 7.38 % and 12.22 % for the minimum and maximum FB stress curves, respectively. For the curve considering the average FB stress, the average error of G_{max} is 1.09 %, representing a very close fit to the experiments. This indicates the feasibility of using average values to predict the effect of fibre bridging to obtain the Paris curve in the steady-state region (fibre bridge saturation).

To conclude, the advantage of the present model is the ability to correct the slope and shift of the SERR from the integration of the fibre bridge stress curve. Additionally, because the fibre bridging effect is added to, or subtracted from, each datapoint individually (see Equations (17) and (18)), the inherent variability of the material (i.e. the variation around the log-linear fit of the Paris curve), is preserved, which is desirable [36].

The minimum requirement for applying the proposed model is one quasi-static test to measure the stress distribution of the fibre bridge and a single fatigue curve. These two tests are sufficient to remove the effect of the fibre bridge or to predict the behaviour of the curve at the steady-state level of fibre bridge saturation. Fig. 3c illustrates the derivation of the zero-bridging curve based a single fatigue curve with the quasi-static test used to generate the average FB stress curve. Also, Fig. 7b shows the estimation of the Paris curve with bridge saturation using a single experimental curve (a-a_0) = 4.98 mm, providing a validation with experimental results. Therefore, the present model can potentially reduce the number of experiments required to characterise mode I fatigue delamination tests and explicitly incorporate the monotonic and cyclic contribution of fibre bridging.

5. Validation and comparison to existing models

In order to validate the proposed model, a comparative analysis between the experimental and other methods presented in the literature is carried out in this section. First, the specimen specific extrapolation method [36] is applied, where a second-order planar relation is applied to the *Log* (G_{max}), *Log (da/dN)* and pre-crack length (a–a_0) data according to Equation (19) [36].

$$Log(G_{max}) = C_0 + C_1(a - a_0) + C_2\, log\left(\frac{da}{dN}\right) + C_3(a - a_0)^2 + C_4\left[log\left(\frac{da}{dN}\right)\right]^2 \tag{19}$$

where, C coefficients represent the fitting constants for each relation.

Changing the pre-crack level to zero (a–a_0 = 0) assumes no fibre bridging occurs [46]. This interpolation makes it possible to generate the curve that removes the effect of fibre bridging. More information on the method can be found in Refs. [36,46,54].

The second model adopted for comparative analysis is the method proposed by Yao et al. [34,35], where the Hartman-Schijve [55] and Jones et al. [56] equation (Equation (20)) is applied.

$$\frac{da}{dN} = \alpha\left[\frac{\Delta\sqrt{G} - \Delta\sqrt{G_{thr}}}{\sqrt{1 - \sqrt{G_{max}}/\sqrt{G_{IC}}}}\right]^{\beta} \tag{20}$$

where, $\Delta\sqrt{G} = \left(\sqrt{G_{max}} - \sqrt{G_{min}}\right)$.

The upper (G_{IC}) and lower (G_{thr}) values of the Paris curve are reduced, considering the elimination of the bridging effect. The linear portion of the Paris curve is then fitted to the new range, assuming no fibre bridge effect. More specifically, to estimate an upper and lower limit for the fatigue curve, $\sqrt{G_{IC,0}}$ (fracture toughness at zero-bridging) and $\sqrt{G_{thr,0}}$ (threshold SERR at zero-bridging) are obtained by plotting the experimental values of both parameters (G_{IC} and G_{thr}) against the corresponding pre-crack extension lengths, a–a_0. By fitting a second-order polynomial curve to these data points, $\sqrt{G_{IC,0}}$ and $\sqrt{G_{thr,0}}$ can be extrapolated by setting the pre-crack extension length to zero [34, 35]. Applying these new values to the Hartman-Schijve equation gives a curve with zero-bridging effect.

The two described models, i.e. the Yao method and specific extrapolation, were used to generate the zero-bridging curve and compared with the curves previously derived with the model proposed in the present paper. Fig. 8 shows the comparative results of an experimental Paris curve (a–a_0 = 2.35 mm) and the zero-bridging curves for each model, highlighting only the Paris fitting. As mentioned above, using minimum fibre bridging effect values cannot guarantee a significant removal of the bridging effect, considering the overlap with the experimental curve. The effect of the maximum FB stress provides the most conservative region of the Paris curve. However, considering that the proposed model is based on an estimate of the energy contribution of the fibre bridge based on an analytical model from the quasi-static FB stress curve, the average region can be considered the most realistic. In fact, the average stress result in a Paris curve shifts similar to the other models available in the literature. This can also be confirmed as a better fit with the literature methods.

Removing the effect of the fibre bridge results in two main changes to the Paris curve. The first is to shift the curve towards lower strain energy values due to the reduction in opening stress. The second is to change the slope of the curve to account for the reduction in stiffness of the material present in the fibre bridge. The proposed method using the average FB stress gives a slope closer to the specific extrapolation model, i.e. a difference of 4.53 %. On the other hand, the proposed model slope shows a difference of 15.63 % with Yao's method. The difference is related to the challenge of determining a specific change in the slope of the curve based on the upper and lower limits in terms of mathematical regression fitting to determine the zero bridge in G_{IC} and G_{thr}.

Table 1 shows the strain energy reduction factors and the difference in the curve slope for each model used in Fig. 8, taking the experimental curve a–a_0 = 2.34 mm as the reference. The fractional reduction in G_{max} values was taken from the average percentage reduction of the entire point-to-point curve. Looking at the effect of the decrease in G_{max} values, the greatest reduction is in the max FB stress, followed by the specific extrapolation method, the Yao method, the average FB stress and, finally, the min FB stress. However, considering that the slope of the curve is modified, this difference in the reduction of G_{max} values becomes dependent on β. This implies a second analysis, which is the effect of changing the slope of the Paris curve. This means a reduction in the material stiffness and the representation of a toughness behaviour of the

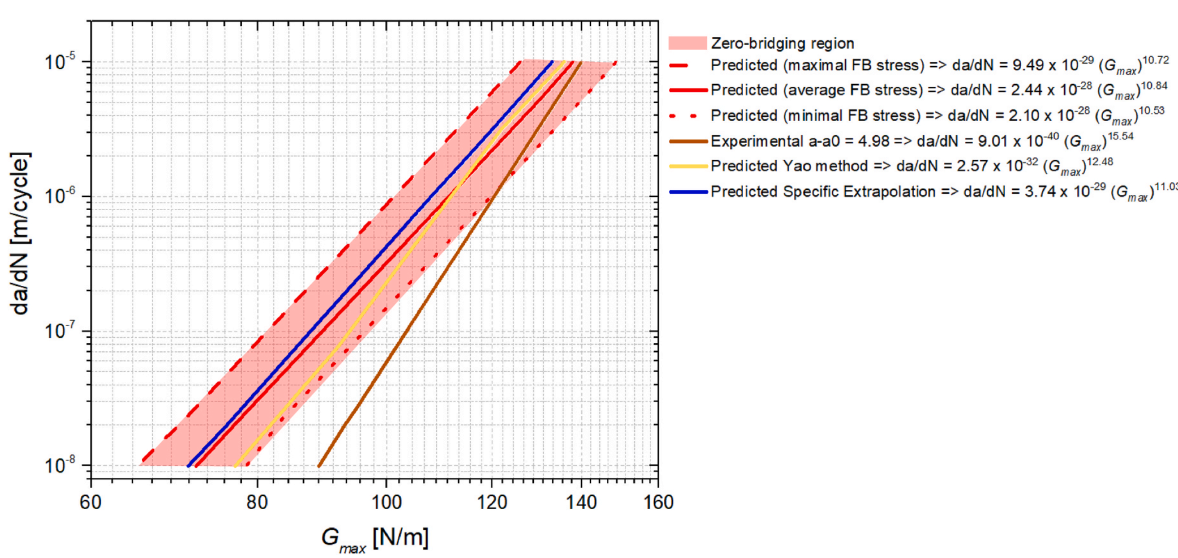

Fig. 8. Comparison analysis of zero-bridging Paris curve.

Table 1
Reduction factor and percentages for proposed models.

Curve	G_{max} Reduction fraction [%]	Slope β	β - Reduction fraction [%]
Exp. Curve (a-a_0 = 2.34 mm)	–	15.24	–
[a]Max FB stress	18.06	10.53	28.87
[a]Aver FB stress	13.19	10.84	30.88
[a]Min FB stress	9.15	10.72	29.65
Yao method	9.33	12.48	18.10
Specific Extrapolation	14.84	11.03	27.64

[a] Considering the maximal, average and minimal fibre bridging (FB) stress curve, respectively.

delamination.

The proposed model shows a higher reduction in the slope of the curve, followed by the specific extrapolation method and with a minor change for the Yao method. The proposed model explicitly measures the cyclic contribution of the FB stress (which is mainly responsible for the change in the slope), whereas the other models make this reduction empirically. This indicates that the proposed model is more sensitive to characterising the effect of reducing the SERR and changing the toughness behaviour to remove the fibre bridging effect. The proposed model can be considered valid for characterising the effect of fibre bridging on the Paris curves.

6. Conclusions

In this study, a novel physical model has been developed and validated to isolate and quantify the contribution of fibre bridging to fatigue strength to fracture. The superposition principle model distinguishes between two components of the SERR contribution of the bridging law on the Paris curve: the monotonic component, which accounts for FB stress from bridging developed during pre-cracking, and a cyclic component, which captures variations during fatigue delamination. The monotonic component is calculated using the Sørensen model, while the cyclic component is derived by integrating a bridging stress function over the end-opening displacement. These functions are interpolated with exponential curves to establish empirical relationships.

The predictions of the model are consistent with the physical behaviour of the double cantilever beam specimen during opening delamination, where removal of the monotonic bridging component from the test mainly contribute to a shift of the Paris curve towards lower SERR values. Removing the cyclic components results also in a reduction in the slope of the Paris curve. The model can also be adapted to estimate the saturation SERR in the Paris curve based on the FB stress from the quasi-static test. This ability of the model was validated experimentally, by predicting the Paris curve for saturated fibre bridging, based on the FB stress curve and a Paris curve with a short pre-crack (lower amount of fibre-bridging). A close match between model prediction and experimental results was observed.

A further validation of the model was carried out in a comparative analysis with existing methods, including the Yao model and the specific extrapolation method. The proposed model showed a greater reduction in the slope of the Paris curve compared to the Yao method, with only minor discrepancies observed when compared to the specific extrapolation method. Unlike these other models, which empirically determine changes in slope, the proposed model explicitly measures the cyclic contribution of fibre bridging stress, making it more sensitive to changes in SERR due to removal of bridging fibres.

In addition, the proposed model only requires a quasi-static test to measure the stress distribution of the fibre bridge and a single fatigue curve. This efficiency suggests that the model can significantly reduce the number of experiments required to characterise mode I fatigue delamination, while providing a detailed account of both the monotonic and cyclic contributions of fibre bridging.

CRediT authorship contribution statement

Francisco Maciel Monticeli: Writing – original draft, Visualization, Methodology, Investigation, Formal analysis, Data curation, Conceptualization. **Davide Biagini:** Writing – review & editing, Validation, Methodology, Formal analysis. **Yasmine Mosleh:** Writing – review & editing, Supervision, Resources, Funding acquisition, Formal analysis. **John-Alan Pascoe:** Writing – review & editing, Supervision, Resources, Project administration, Funding acquisition.

Declaration of competing interest

The authors disclose to have no financial and personal relationships with other people or organizations that could inappropriately influence their work.

Acknowledgements

The research was funded by the European Union under GA No. 101091409 (D-STANDART). Views and opinions expressed are however those of the author(s) only and do not necessarily reflect those of the European Union. Neither the European Union nor the granting authority can be held responsible for them.

Data availability

The data underlying this work is publicly available via a Zenodo repository: 10.5281/zenodo.14831359

References

[1] Pereira AB, Morais AB De. SCIENCE AND Mode II interlaminar fracture of carbon/epoxy multidirectional laminates, vol. 64; 2004. p. 1653–9. https://doi.org/10.1016/j.compscitech.2003.12.001.
[2] Russo A, Riccio A, Palumbo C, Sellitto A. Fatigue driven delamination in composite structures: definition and assessment of a novel fracture mechanics based computational tool. Int J Fatig 2023;166:107257. https://doi.org/10.1016/j.ijfatigue.2022.107257.
[3] Zhang Y, Vassilopoulos AP, Keller T. Mode I and II fracture behavior of adhesively-bonded pultruded composite joints. Eng Fract Mech 2010;77:128–43. https://doi.org/10.1016/j.engfracmech.2009.09.015.
[4] Charalambous G, Allegri G, Lander JK, Hallett SR. A cut-ply specimen for the mixed-mode fracture toughness and fatigue characterisation of FRPs. Compos Part A Appl Sci Manuf 2015;74:77–87. https://doi.org/10.1016/j.compositesa.2015.02.020.
[5] Carreras L, Bak BLV, Jensen SM, Lequesne C, Xiong H, Lindgaard E. Benchmark test for mode I fatigue-driven delamination in GFRP composite laminates: experimental results and simulation with the inter-laminar damage model implemented in SAMCEF. Compos Part B Eng 2023;253:110529. https://doi.org/10.1016/j.compositesb.2023.110529.
[6] Khan R. Fiber bridging in composite laminates: a literature review. Compos Struct 2019;229. https://doi.org/10.1016/j.compstruct.2019.111418.
[7] Yao L, Liu J, Lyu Z, Alderliesten RC, Hao C, Ren C, et al. In-situ damage mechanism investigation and a prediction model for delamination with fibre bridging in composites. Eng Fract Mech 2023;281:109079. https://doi.org/10.1016/j.engfracmech.2023.109079.
[8] Hu P, Pulungan D, Tao R, Lubineau G. An experimental study on the influence of intralaminar damage on interlaminar delamination properties of laminated composites. Compos Part A Appl Sci Manuf 2020;131:105783. https://doi.org/10.1016/j.compositesa.2020.105783.
[9] Saeedifar M, Ahmadi Najafabadi M, Mohammadi K, Fotouhi M, Hosseini Toudeshky H, Mohammadi R. Acoustic emission-based methodology to evaluate delamination crack growth under quasi-static and fatigue loading conditions. J Nondestruct Eval 2018;37:1–13. https://doi.org/10.1007/s10921-017-0454-0.
[10] Shor O, Banks-Sills L, Simon I. Quasi-static modes I, II and mixed modes I/II fracture toughness of two laminate composites: Part II — micro-computerized tomography and numerical simulations. Eng Fract Mech 2023;277:108976. https://doi.org/10.1016/j.engfracmech.2022.108976.
[11] Silversides I, Maslouhi A, LaPlante G. Acoustic emission monitoring of interlaminar delamination onset in carbon fibre composites. Struct Health Monit 2013;12:126–40. https://doi.org/10.1177/1475921712469994.
[12] Nikbakht M, Yousefi J, Hosseini-Toudeshky H, Minak G. Delamination evaluation of composite laminates with different interface fiber orientations using acoustic emission features and micro visualization. Compos Part B Eng 2017;113:185–96. https://doi.org/10.1016/j.compositesb.2016.11.047.

[13] Maneval V, Vedvik NP, Echtermeyer AT. Progressive fatigue modelling of open-hole glass-fibre epoxy laminates. J Compos Sci 2023;7. https://doi.org/10.3390/jcs7120516.
[14] Erives R, Sørensen BF, Goutianos S. Extraction of mix-mode cohesive laws of a unidirectional composite undergoing delamination with large-scale fibre bridging. Compos Part A Appl Sci Manuf 2023;165:107346. https://doi.org/10.1016/j.compositesa.2022.107346.
[15] Gribniak V, Sokolov A. Standardized RC beam tests for modeling the fiber bridging effect in SFRC. Constr Build Mater 2023;370:130652. https://doi.org/10.1016/j.conbuildmat.2023.130652.
[16] ASTM D6115-97. Standard test method for mode I fatigue delamination growth onset of unidirectional fiber-reinforced polymer matrix composites. Am Stand Test Methods 2019;1:1–7.
[17] Yao L, Cui H, Sun Y, Guo L, Chen X, Zhao M, et al. Fibre-bridged fatigue delamination in multidirectional composite laminates. Compos Part A Appl Sci Manuf 2018;115:175–86. https://doi.org/10.1016/j.compositesa.2018.09.027.
[18] Jiang L, Zhang Y, Gong Y, Li W, Ren S, Liu H. A new model characterizing the fatigue delamination growth in DCB laminates with combined effects of fiber bridging and stress ratio. Compos Struct 2021;268:113943. https://doi.org/10.1016/j.compstruct.2021.113943.
[19] Tian D, Gong Y, Gao Y, Zou L, Zhang J, Zhao L, et al. Numerical modelling of the mode I fracture behavior in composite laminates with significant R-curve effect. Theor Appl Fract Mech 2023;128:104172. https://doi.org/10.1016/j.tafmec.2023.104172.
[20] Zhang AY, Liu HY, Mouritz AP, Mai YW. Experimental study and computer simulation on degradation of z-pin reinforcement under cyclic fatigue. Compos Part A Appl Sci Manuf 2008;39:406–14. https://doi.org/10.1016/j.compositesa.2007.09.006.
[21] Sorensen L, Botsis J, Gmür T, Humbert L. Bridging tractions in mode I delamination: measurements and simulations. Compos Sci Technol 2008;68:2350–8. https://doi.org/10.1016/j.compscitech.2007.08.024.
[22] Kaute DAW, Shercliff HR, Ashby MF. Delamination, fibre bridging and toughness of ceramic matrix composites. Acta Metall Mater 1993;41:1959–70. https://doi.org/10.1016/0956-7151(93)90366-Z.
[23] Sørensen BF, Gamstedt EK, Østergaard RC, Goutianos S. Micromechanical model of cross-over fibre bridging - prediction of mixed mode bridging laws. Mech Mater 2008;40:220–34. https://doi.org/10.1016/j.mechmat.2007.07.007.
[24] Daneshjoo Z, Shokrieh MM, Fakoor M. A micromechanical model for prediction of mixed mode I/II delamination of laminated composites considering fiber bridging effects A micromechanical model for prediction of mixed mode I/II delamination of laminated composites considering fi ber bridgin. Theor Appl Fract Mech 2018;94:46–56. https://doi.org/10.1016/j.tafmec.2017.12.002.
[25] Monticeli FM, Odila Hilário Cioffi M, Jacobus Cornelis Voorwald H. The influence of carbon/glass/epoxy hybrid composite under mode I fatigue loading: hybrid fiber bridging zone model. Compos Struct 2022;286:115274. https://doi.org/10.1016/j.compstruct.2022.115274.
[26] Joosten MW, Dávila CG, Yang Q. Predicting fatigue damage in composites subjected to general loading conditions. Compos Part A Appl Sci Manuf 2022;156. https://doi.org/10.1016/j.compositesa.2022.106862.
[27] Dávila CG, Weeks S, Czabaj M. Propagation rate transients in J-controlled fatigue characterization of adhesives. Int J Fatig 2024;185. https://doi.org/10.1016/j.ijfatigue.2024.108377.
[28] Stutz S, Cugnoni J, Botsis J. Studies of mode I delamination in monotonic and fatigue loading using FBG wavelength multiplexing and numerical analysis. Compos Sci Technol 2011;71:443–9. https://doi.org/10.1016/j.compscitech.2010.12.016.
[29] Teimouri F, Heidari-Rarani M, Haji Aboutalebi F. Finite element modeling of mode I fatigue delamination growth in composites under large-scale fiber bridging. Compos Struct 2021;263:113716. https://doi.org/10.1016/j.compstruct.2021.113716.
[30] Hu X, Wittmann F. Ternal loading and the bridging region . This definition of the fracture-process zone is the same as that of the fictitious crack model initiated by Hillerborg. J Mater Civ Eng 1990;2:15–23.
[31] Khan R, Alderliesten R, Yao L, Benedictus R. Crack closure and fibre bridging during delamination growth in carbon fibre/epoxy laminates under mode I fatigue loading. Compos Part A 2014;67:201–11.
[32] Banks-Sills L, Ben Gur H. The effect of fiber bridging on mode I fatigue delamination propagation—part I: testing. Fatig Fract Eng Mater Struct 2024:1–17. https://doi.org/10.1111/ffe.14362.
[33] Dávila CG, Rose CA, Camanho PP. A procedure for superposing linear cohesive laws to represent multiple damage mechanisms in the fracture of composites. Int J Fract 2009;158:211–23. https://doi.org/10.1007/s10704-009-9366-z.
[34] Yao L, Alderliesten R, Zhao M, Benedictus R. Bridging effect on mode i fatigue delamination behavior in composite laminates. Compos Part A Appl Sci Manuf 2014;63:103–9. https://doi.org/10.1016/j.compositesa.2014.04.007.
[35] Yao L, Sun Y, Guo L, Zhao M, Jia L, Alderliesten RC, et al. A modified Paris relation for fatigue delamination with fibre bridging in composite laminates. Compos Struct 2017;176:556–64. https://doi.org/10.1016/j.compstruct.2017.05.070.
[36] Alderliesten R. Fatigue delamination of composite materials - approach to exclude large scale fibre bridging. IOP Conf Ser Mater Sci Eng 2018;388:012002. https://doi.org/10.1088/1757-899X/388/1/012002.
[37] ASTM D5528. Standard test method for mode I interlaminar fracture toughness of unidirectional fiber-reinforced polymer matrix composites. Am Soc Test Mater 2021;1:1–14. https://doi.org/10.1520/D5528_D5528M-21.
[38] ASTM D6115. Standard test method for mode I fatigue delamination growth onset of unidirectional fiber-reinforced polymer matrix composites. Am Soc Test Mater 2019;1:1–7. https://doi.org/10.1520/D6115-97R19.
[39] Sørensen BF, Jacobsen TK. Large-scale bridging in composites: R-curves and bridging laws. Compos Part A Appl Sci Manuf 1998;29:1443–51. https://doi.org/10.1016/S1359-835X(98)00025-6.
[40] Tauheed M, Datla NV. Mode I fracture R-curve and cohesive law of CFRP composite adhesive joints. Int J Adhesion Adhes 2022;114:103102. https://doi.org/10.1016/j.ijadhadh.2022.103102.
[41] Fleck NA, Sutcliffe MPF, Sivashanker S, Xin XJ. Compressive R-curve of a carbon fibre-epoxy matrix composite. Compos Part B Eng 1996;27:531–41. https://doi.org/10.1016/1359-8368(95)00037-2.
[42] Jacobsen TK, Sørensen BF. Mode I intra-laminar crack growth in composites - modelling of R-curves from measured bridging laws. Compos Part A Appl Sci Manuf 2001;32:1–11. https://doi.org/10.1016/S1359-835X(00)00139-1.
[43] Alderliesten RC, Brunner AJ, Pascoe JA. Cyclic fatigue fracture of composites: what has testing revealed about the physics of the processes so far? Eng Fract Mech 2018;203:186–96. https://doi.org/10.1016/j.engfracmech.2018.06.023.
[44] Ciavarella M, Monno F. On the possible generalizations of the Kitagawa-Takahashi diagram and of the El Haddad equation to finite life. Int J Fatig 2006;28:1826–37. https://doi.org/10.1016/j.ijfatigue.2005.12.001.
[45] Brunner AJ, Alderliesten R, Pascoe J. In-service delaminations in FRP structures under operational loading conditions: are current fracture testing and analysis on coupons sufficient for capturing the essential effects for reliable predictions? Materials 2023;16:1–24.
[46] Yao L, Alderliesten RC, Benedictus R. The effect of fibre bridging on the Paris relation for mode I fatigue delamination growth in composites. Compos Struct 2016;140:125–35. https://doi.org/10.1016/j.compstruct.2015.12.027.
[47] van der Panne M, Pascoe JA. Fatigue delamination growth - is UD testing enough? Procedia Struct Integr 2022;42:449–56. https://doi.org/10.1016/j.prostr.2022.12.057.
[48] Tamuzs V, Tarasovs S, Vilks U. Progressive delamination and fiber bridging modeling in double cantilever beam composite specimens. Eng Fract Mech 2001;68:513–25. https://doi.org/10.1016/S0013-7944(00)00131-4.
[49] Duan Q, Hu H, Cao D, Cai W, Li S. A new mechanism based cohesive zone model for Mode I delamination coupled with fiber bridging of composite laminates. Compos Struct 2024;332. https://doi.org/10.1016/j.compstruct.2024.117931.
[50] Monticeli FM, Voorwald HJC, Cioffi MOH. The influence of carbon-glass/epoxy hybrid composite under mode I fatigue loading: physical-based characterization. Compos Struct 2022;286. https://doi.org/10.1016/j.compstruct.2022.115291.
[51] Pascoe JA, Alderliesten RC, Benedictus R. Characterising resistance to fatigue crack growth in adhesive bonds by measuring release of strain energy. Procedia Struct Integr 2016;2:80–7. https://doi.org/10.1016/j.prostr.2016.06.011.
[52] Pascoe JA, Alderliesten RC, Benedictus R. Methods for the prediction of fatigue delamination growth in composites and adhesive bonds - a critical review. Eng Fract Mech 2013;112–113:72–96. https://doi.org/10.1016/j.engfracmech.2013.10.003.
[53] Feih S, Wei J, Kingshott P, Sørensen BF. The influence of fibre sizing on the strength and fracture toughness of glass fibre composites. Compos Part A Appl Sci Manuf 2005;36:245–55. https://doi.org/10.1016/j.compositesa.2004.06.019.
[54] Murri GB. Effect of data reduction and fiber-bridging on Mode i delamination characterization of unidirectional composites. J Compos Mater 2014;48:2413–24. https://doi.org/10.1177/0021998313498791.
[55] Hartman A, Schijve J. The effects of environment and load frequency on the crack propagation law for macro fatigue crack growth in aluminium alloys. Eng Fract Mech 1970;1:615–31. https://doi.org/10.1016/0013-7944(70)90003-2.
[56] Jones R, Kinloch AJ, Michopoulos JG, Brunner AJ, Phan N. Delamination growth in polymer-matrix fibre composites and the use of fracture mechanics data for material characterisation and life prediction. Compos Struct 2017;180:316–33. https://doi.org/10.1016/j.compstruct.2017.07.097.